Informatics 2019, IEEE proceedings,pp.363-368, ISBN 978-1-7281-3178-8, Poprad, Slovakia, 2019

Reconstruction of Corrupted Vector Fields using Radial Basis Functions

Michal Smolik
Department of Computer Science and Engineering
Faculty of Applied Sciences, University of West Bohemia
Plzen, Czech Republic
smolik@kiv.zcu.cz

Vaclav Skala
Department of Computer Science and Engineering
Faculty of Applied Sciences, University of West Bohemia
Plzen, Czech Republic
skala@kiv.zcu.cz

***Abstract*—The vector fields may be results from the measurements of real flow experiments. However, during the measurements, some parts of the vector field can be measured incorrectly or even some parts of the vector field are not possible to capture due to some shading and invisibility. In this paper, we focus on the reconstruction of such corrupted vector fields. We detect the locations, where the vector field was measured incorrectly and reconstruct those locations of the vector field. For the reconstruction, we use Radial Basis Functions (RBF) approximation to fill the missing locations of the vector field as well as to correct and smooth the locations of the vector field, where it was probably measured with some error. The results of the proposed method are presented in this paper.**

***Index Terms*—Vector field, reconstruction, Radial basis functions, corrupted data, approximation.**

I. Introduction

The interpolation and approximation are probably the most frequent operations used in computational methods. Several methods have been developed for data interpolation and approximation, but they expect some kind of data "ordering", e.g. structured mesh, rectangular mesh, unstructured mesh, etc. However, in many engineering problems, data are not ordered and they are scattered in $d-$dimensional space, in general. Usually, in technical applications, the scattered data are tessellated using triangulation but this approach is quite prohibitive for the case of $d-$dimensional data interpolation because of the computational cost.

Interpolated and approximated scattered vector data on a surface become frequent in applied problem solutions. There are applications for vector field decomposition [1], for vector field design system for surfaces that allows the user to control the number of singularities in the vector field and their placement [2]. The paper [3] uses the vector field interpolation for estimating robust point correspondences between two sets of points. An approach for critical points reduction and vector field approximation using Radial basis functions is presented in [4] with an extension into $3D$ in [5].

Vector fields can be measured during experiments. However, the accuracy of measurements is sometimes low and sometimes part of the vector field cannot be measured due to obstacle and invisibility of the vector field. There exist some methods that deal with this problem. The paper [6] presents an approach for reconstruction of vector field. Another approach is presented in [7]. The paper [8] presents an approach for reconstruction of wind field from limited information provided by a lidar system. This approach is able to reconstruct complex situations. The follow-up paper [9] presents the possibility of using nacelle-mounted lidar for wind field reconstruction. The reconstruction of $2D$ vector field from sparse set of points-vectors pairs is presented in [10]. The approach subdivides the domain adaptively in order to make local piece-wise polynomial approximations for the field. After that, it uses the partition of unity to blend the local approximations together. A method for the global vector-field reconstruction of nonlinear dynamical systems from a time series is studied in the paper [11]. It employs a complete set of polynomials and singular value decomposition to estimate a standard function, which is central to the algorithm. The paper [12] presents a method for the reconstruction of flow fields based on adaptive control grid interpolation. The data for reconstruction are acquired from the magnetic resonance and the resulting velocity field is with high quality. The paper [13] aims to show that it is possible to accurately estimate, in a real-time fashion, the radial and tangential velocity components of the wind field from lidar data. The reconstruction is generated through the synthesis of an unscented Kalman filter that employs a low-order dynamic model of the wind to estimate the unmeasured velocities within the wind field, using repeated measurement updates from typical nacelle-mounted lidar instruments. Another approach for reconstruction of vector fields is presented in [14]. This paper focuses on reconstruction of tomography data sets.

In this paper, we present a new approach for reconstruction of incomplete or corrupted vector fields using Radial Basis Functions (RBF).

II. Vector field

Vector fields on surfaces are important objects, which appear frequently in scientific simulation in CFD (Computational Fluid Dynamics) or modeling by FEM (Finite Element Method). To be visualized, such vector fields are usually lin-

The authors would like to thank their colleagues at the University of West Bohemia, Plzen, for their discussions and suggestions. The research was supported by projects Czech Science Foundation (GACR) No. GA17-05534S and partially by SGS 2019-016.

early approximated for the sake of simplicity and performance considerations.

The vector field can be easily analyzed when having an approximation of the vector field near some location point. The important places to be analyzed are so called critical points. Analyzing the vector field behavior near these points gives us the information about the characteristic of the vector field.

A. Critical Point

Critical points $\boldsymbol{x}_0$ of the vector field are points at which the magnitude of the vector vanishes

$$\frac{d\boldsymbol{x}}{dt} = \boldsymbol{v}(\boldsymbol{x}) = \boldsymbol{0}, \tag{1}$$

i.e. all components are equal to zero

$$\begin{bmatrix} \frac{dx}{dt} \\ \frac{dy}{dt} \end{bmatrix} = \begin{bmatrix} 0 \\ 0 \end{bmatrix}. \tag{2}$$

A critical point is said to be isolated, or simple, if the vector field is non vanishing in an open neighborhood around the critical point. Thus for all surrounding points $\boldsymbol{x}_\epsilon$ of the critical point $\boldsymbol{x}_0$ the equation (1) does not apply, i.e.

$$\frac{d\boldsymbol{x}_\epsilon}{dt} \neq \boldsymbol{0}, \tag{3}$$

At critical points, the direction of the field line is indeterminate, and they are the only points in the vector field were field lines can intersect (asymptotically). The terms singular point, null point, neutral point or equilibrium point are also frequently used to describe critical points.

These points are important because together with the nearby surrounding vectors, they have more information encoded in them than any such group in the vector field, regarding the total behavior of the field, see Fig. 1.

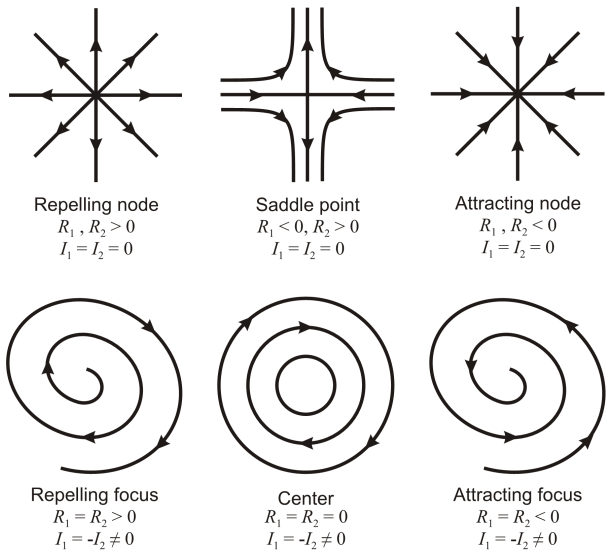

Fig. 1. Classification of $2D$ first order critical points. R_1, R_2 denote the real parts of the eigenvalues of the Jacobian matrix while I_1, I_2 denote their imaginary parts.

III. Radial Basis Functions

The Radial basis functions (RBF) is a technique for scattered data interpolation [15], [16] and approximation [17], [18]. The RBF interpolation and approximation is computationally more expensive, because input data are not ordered and there is no known relation between them. Although the RBF has higher computational cost, it can be used for d-dimensional problem solution in many applications, e.g. solution of partial differential equations, image reconstruction, neural networks, fuzzy systems, GIS systems, optics etc.

The RBF is a function whose value depends only on the distance from some center point. Due to the use of the distance functions, the RBFs can be easily implemented to reconstruct the surface using scattered data in $2D$, $3D$ or higher dimensional spaces. It should be noted that the RBF approximation is not separable.

The RBF interpolation was originally introduced by [19] and is based on computing the distance of two points in the k-dimensional space and is defined by a function

$$f(\boldsymbol{x}) = \sum_{j=1}^{M} \lambda_j \varphi(\|\boldsymbol{x} - \boldsymbol{x}_j\|) \tag{4}$$

where λ_j are weights of the RBFs, M is the number of the radial basis functions, i.e. the number of interpolation points, and φ is the radial basis function. For a given dataset of points with associated values, i.e. in the case of scalar values $\{\boldsymbol{x}_i, h_i\}_1^M$, the following linear system of equations is obtained

$$h_i = f(\boldsymbol{x}_i) = \sum_{j=1}^{M} \lambda_j \varphi(\|\boldsymbol{x}_i - \boldsymbol{x}_j\|) \quad \text{for } \forall i \in \{1, \ldots, M\} \tag{5}$$

where λ_j are weights to be computed.

Equation (5) can be rewritten in a matrix form as

$$\boldsymbol{A}\boldsymbol{\lambda} = \boldsymbol{h}, \tag{6}$$

where matrix $\boldsymbol{A}$ is symmetrical, as $\|\boldsymbol{x}_i - \boldsymbol{x}_j\| = \|\boldsymbol{x}_j - \boldsymbol{x}_i\|$.

Radial function interpolants have a nice property of being invariant under all Euclidean transformations, i.e. translations, rotations and reflections. It means that it does not matter whether we first compute the RBF interpolation function and then apply a Euclidean transformation, or if we first transform all the data and then compute the radial function interpolants. This is result of the fact that Euclidean transformations are characterized by orthogonal transformation matrices and are therefore 2 norm invariant. Radial basis functions can be

divided into two groups according to their influence. First group are "global" RBF [20], for example:

$$\begin{aligned}
\text{Thin Plate Spline (TPS)} \quad & \varphi(r) = r^2 \log r \\
\text{Gauss function} \quad & \varphi(r) = e^{-(\epsilon r)^2} \\
\text{Inverse Quadric (IQ)} \quad & \varphi(r) = \frac{1}{1+(\epsilon r)^2} \\
\text{Inverse Multiquadric (IMQ)} \quad & \varphi(r) = \frac{1}{\sqrt{1+(\epsilon r)^2}} \\
\text{Multiquadric (MQ)} \quad & \varphi(r) = \sqrt{1+(\epsilon r)^2}
\end{aligned} \tag{7}$$

where ϵ is the shape parameter of radial basis function [21].

The "local" RBF were introduced by [22] as Compactly Supported RBF (CSRBF) and satisfy the following condition

$$\varphi(r) = (1-r)_+^q P(r) = \begin{cases} (1-r)^q P(r) & 0 \le r \le 1 \\ 0 & r > 1 \end{cases} \tag{8}$$

where $P(r)$ is a polynomial function and q is a parameter. Typical examples of CSRBF are

$$\begin{aligned}
\varphi_1(r) &= (1-\epsilon r)_+ \\
\varphi_2(r) &= (1-\epsilon r)_+^3 (3\epsilon r + 1) \\
\varphi_3(r) &= (1-\epsilon r)_+^5 (8(\epsilon r)^2 + 5\epsilon r + 1) \\
\varphi_4(r) &= (1-\epsilon r)_+^2 \\
\varphi_5(r) &= (1-\epsilon r)_+^4 (4\epsilon r + 1) \\
\varphi_6(r) &= (1-\epsilon r)_+^6 (35(\epsilon r)^2 + 18\epsilon r + 3) \\
\varphi_7(r) &= (1-\epsilon r)_+^8 (32(\epsilon r)^3 + 25(\epsilon r)^2 + 8\epsilon r + 1) \\
\varphi_8(r) &= (1-\epsilon r)_+^3 \\
\varphi_9(r) &= (1-\epsilon r)_+^3 (5\epsilon r + 1) \\
\varphi_{10}(r) &= (1-\epsilon r)_+^7 (16(\epsilon r)^2 + 7\epsilon r + 1)
\end{aligned} \tag{9}$$

where ϵ is the shape parameter of radial basis function, see Figure 2 for visualization of (9).

The RBF interpolation can be done using "global" or "local" functions. When using "global" radial basis functions the matrix $\boldsymbol{A}$ will be full, but when using "local" radial basis functions the matrix $\boldsymbol{A}$ will be sparse, which can be beneficial when solving the system of linear equations $\boldsymbol{A\lambda} = \boldsymbol{h}$.

In the case of the vector data, i.e. $\{\boldsymbol{x}_i, \boldsymbol{h}_i\}_1^M$ values $\boldsymbol{h}_i$ are actually vectors, the RBF is to be performed for each coordinate of $\boldsymbol{h}_i$.

IV. Proposed approach

The purpose of this approach is to reconstruct the measured vector field. During the measurements, there can be some errors, inaccuracies or even some parts of the vector field can be missing. We will consider the flow around a cylinder in the proposed approach[1].

In the first step, we need to locate the missing parts of the vector field. During the measurement, we obtain several vector fields in different timestamps. From all of this vector fields for

[1]Data courtesy of Rut Vitkovicova, CTU in Prague, FME, Department of Fluid Dynamics and Thermodynamics, Technická 4, 166 07 Prague, Czech Republic [24].

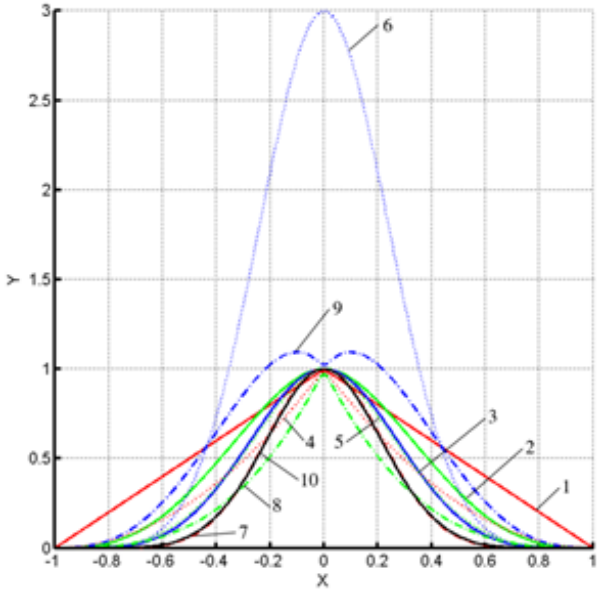

Fig. 2. Examples of CSRBF (from [23]).

different timestamps, we can compute the average speed of the vector field at every location. The parts, where the average speed is low, are measured incorrectly, as the average speed at each location should be similar as we are considering the flow around a cylinder. An example of the computed average speed of the vector field is visualized in Fig. 3. It can be seen, that the low average speed is located at the inflow location on the right side and below the cylinder, where the flow is over-shaded with the cylinder.

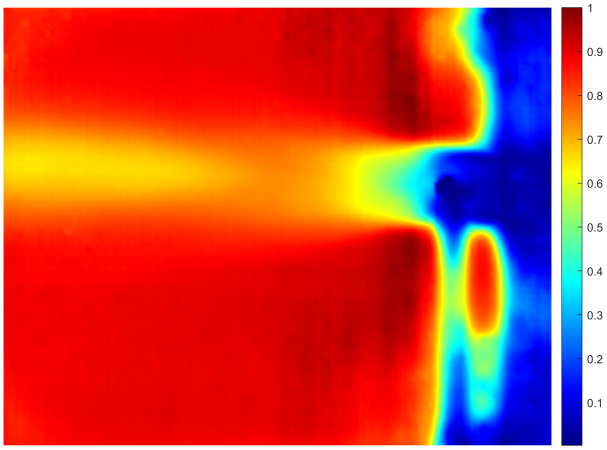

Fig. 3. Average speed of the vector field over simulation time. The color-bar is in relative units [%].

To determine the exact location of incorrectly measured vector field, we need to select some threshold value for the average speed. During the experiments, we determined that the vectors with speed $\le 30\%$ of the maximal average speed are taken as unmeasured or faulty. The vectors with speed in the interval $(30\%, 50\%)$ may be affected by error. The vectors

with speed $\geq 50\%$ are taken as correct, see Fig. 4.

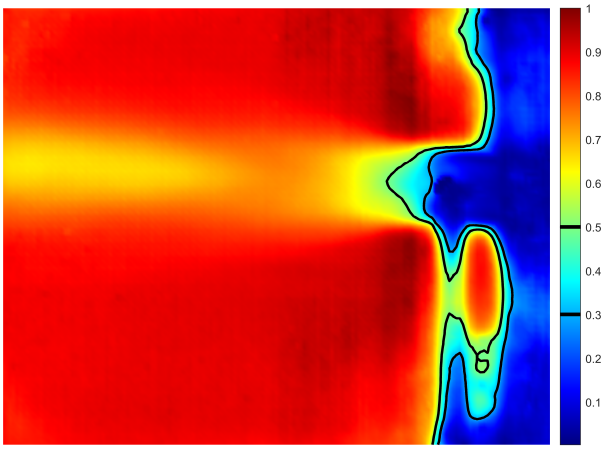

Fig. 4. Average speed of vector field over simulation time with marked contours for 30% and 50% of the maximal average speed. The vectors with speed $\leq 30\%$ are taken as unmeasured or faulty. The vectors with speed in the interval $(30\%, 50\%)$ may be affected by error. The vectors with speed $\geq 50\%$ are taken as correct.

The correctly measured parts of vector field should be preserved during the reconstruction of corrupted vector field. On the opposite site, the unmeasured or faulty parts of the vector field should be totally removed and replaced with data extrapolation. The vectors from locations, where it is not clearly possible to determine the accuracy of the measured vector field data, can be slightly modified.

To fulfill the requirements described before, we use the approximation method of Radial basis functions. The standard vector field approximation with RBF uses the following equations

$$\boldsymbol{v}_i = v(\boldsymbol{x}_i) = \sum_{j=1}^{M} \boldsymbol{\lambda}_j \varphi(\|\boldsymbol{x}_i - \boldsymbol{\xi}_j\|) \quad \text{for } \forall i \in \{1, \ldots, N\}, \quad (10)$$

where $\boldsymbol{v}_i = [v_i^{(x)}, v_i^{(y)}]^T$ is the vector at $\boldsymbol{x}_i$, $\boldsymbol{\lambda}_j = [\lambda_j^{(x)}, \lambda_j^{(y)}]$ is the RBF weight to be computed and $\boldsymbol{\xi}_j$ is the center of the radial basis function.

All the equations (11) forming the system of linear equations have the same importance in the standard RBF approximation. However, we can change the importance or weight of each equation separately. If we multiply one of the equations in (11) as the following

$$\beta_i \boldsymbol{v}_i = \sum_{j=1}^{M} \boldsymbol{\lambda}_j \beta_i \varphi(\|\boldsymbol{x}_i - \boldsymbol{\xi}_j\|) \quad \text{for } i \in \{1, \ldots, N\}, \quad (11)$$

we end up with the weighted vector field RBF approximation.

If all the coefficients are equal to one, i.e. $\forall i : \beta_i = 1$, then it is as the standard RBF approximation. If we multiply one equation with $\beta_i > 1$, then the i^{th} equation has higher importance, as during the approximation the i^{th} error is multiplied with number higher than one. The approximation tries to increase the importance at that location and thus approximates the vector field more correctly at $\boldsymbol{x}_i$ than at other locations (with $\beta_i = 1$). On the opposite side, if we multiply one equation with $0 < \beta_i < 1$, then the i^{th} equation has lower importance, as during the approximation the i^{th} error is multiplied with number smaller than one. Thus, the approximation can differ a bit more at $\boldsymbol{x}_i$ compared to other locations.

In the proposed approach for a vector field reconstruction, we use the above described weighted vector field RBF approximation. We have defined three types of locations, see Fig. 4. The location with unmeasured or faulty vector field is not used during the vector field approximation. The location with correct vector field is used in the RBF approximation and has the weight $\beta_i = 1$.

The last part of the vector field, that can be affected by error has the weight $\beta_i \in (0, 1)$. To compute the exact value of β_i, we use the following formula

$$\beta_i = \frac{speed_i - speed_{START}}{speed_{END} - speed_{START}}, \quad (12)$$

where $speed_i$ is the average speed of the vector field at location $\boldsymbol{x}_i$, $speed_{START}$ is 30% of the maximal average speed and $speed_{END}$ is 50% of the maximal average speed.

Using this approach, we can compute the RBF approximation of corrupted vector field. However, in the case of Fig. 3, we have no data in the right part of the vector field. This is the inflow location, where the vector field has the direction vectors pointing from left to right. We can use this information and add those vectors at the starting border of the vector field. The speed of the starting vectors is selected as the average speed of all correctly measure vectors.

V. Experimental results

The proposed approach for reconstruction of corrupted vector fields was tested on several measured vector fields. We already presented the result of the average speed of the vector field over the simulation time, see Fig. 3. For the vector field RBF approximation, we used the local radial basis function with the following formula

$$\varphi_5(r) = (1 - \epsilon r)_+^4 (4\epsilon r + 1). \quad (13)$$

Using the computed average speed (Fig. 3) and our proposed approach, we reconstructed the vector field Fig. 5a. The result after the reconstruction using the proposed approach is visualized in Fig. 5b. It can be seen that the reconstructed vector field has the same important characteristics as the original vector field. The inflow of the vector field has the correct direction beside the direction of the measured inflow vector field.

The computed average speed (Fig. 3), which is used to determine different types of measured vector field (measured correctly, measured incorrectly and measured with possible error) is used for all timestamps of the vector field. Thus when performing the reconstruction of corrupted vector field, the

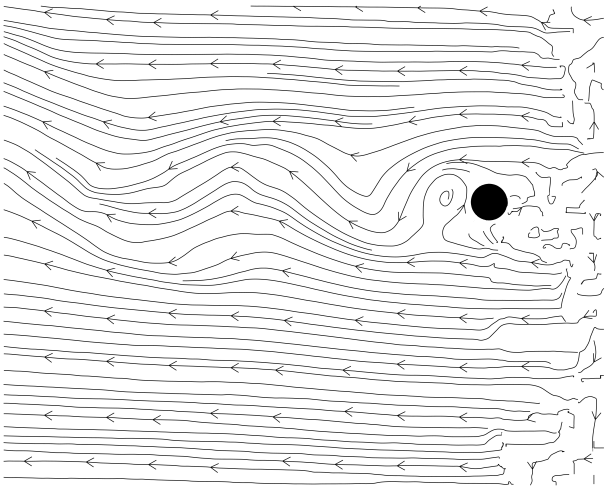

(a) Measured vector field.

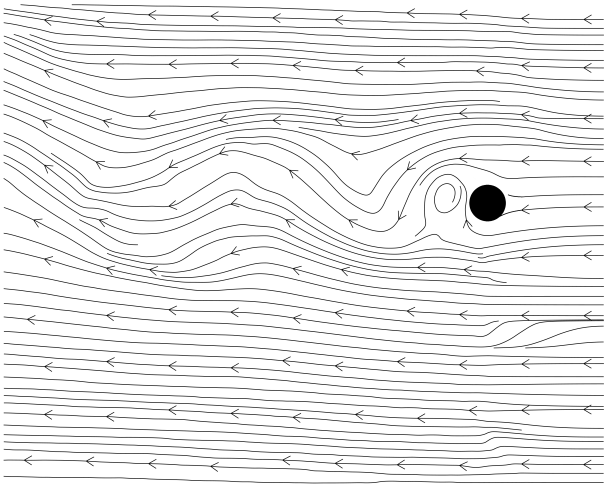

(b) Reconstructed vector field.

Fig. 5. Visualization of measured vector field from the experiment (a) and the corrected vector field with reconstructed missing or error parts (b). Simulation time of this vector field is 5.5 $[s]$.

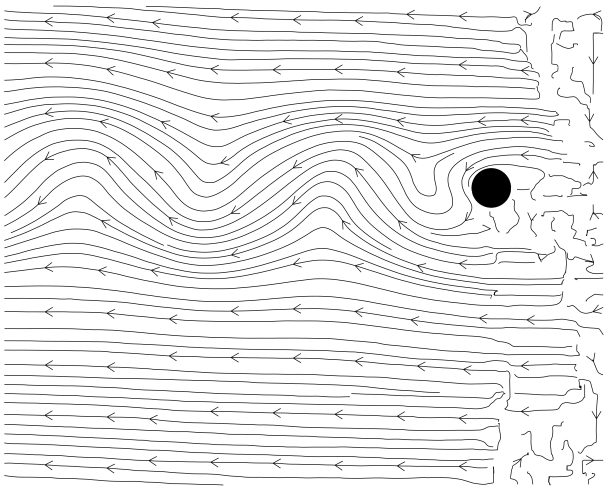

(a) Measured vector field.

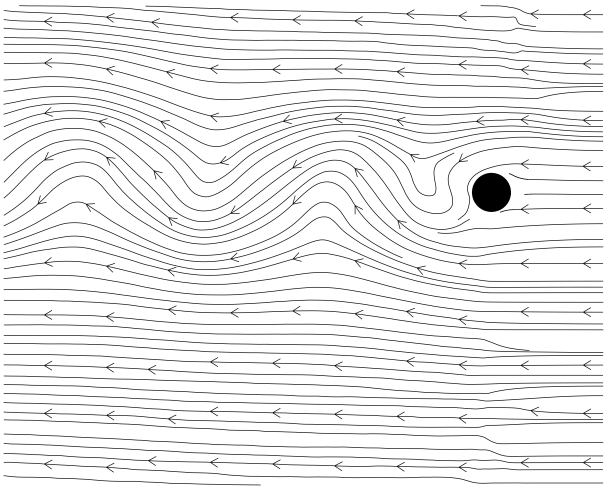

(b) Reconstructed vector field.

Fig. 6. Visualization of measured vector field from the experiment (a) and the corrected vector field with reconstructed missing or error parts (b). Simulation time of this vector field is 37 $[s]$.

average vector field is computed only once and used for all timestamps of the vector field.

Another result of the proposed approach is visualized in Fig. 6b. This result is the reconstruction of a measured vector field (Fig. 6a) at different time than the previous vector field (Fig. 5a).

It can be seen, that the vector field reconstruction result is visually correct as the previous example. The proposed approach can be used to reconstruct the missing parts of the measured vector field or to correct incorrectly measured parts of the vector field.

VI. Conclusion

We presented a new approach for reconstruction of measured vector fields. The approach reconstructs the missing parts of the vector field and is able to correct incorrectly measured parts of the vector field. As the first step of the proposed approach, we presented an approach to detect incorrectly or faulty measured parts of the vector field that need to be corrected or reconstructed. For the final reconstruction, we use the introduced weighted Radial basis function approximation method. The presented results proved the ability to reconstruct and correct the measured vector fields.

In the feature, we plan to develop even more sophisticated method for detection of incorrectly measured parts of the vector field as well as the extension of the proposed approach to $3D$.

Acknowledgment

The authors would like to thank their colleagues at the University of West Bohemia, Plzen, for their discussions and suggestions. The research was supported by projects Czech Science Foundation (GACR) No. GA17-05534S and partially by SGS 2019-016.

REFERENCES

[1] G. B. W. Edward J. Fuselier, "Stability and error estimates for vector field interpolation and decomposition on the sphere with rbfs," *SIAM Journal on Numerical Analysis*, vol. 47, no. 5, pp. 3213–3239, 2009.

[2] E. Zhang, K. Mischaikow, and G. Turk, "Vector field design on surfaces," *ACM Trans. Graph.*, vol. 25, no. 4, pp. 1294–1326, 2006. [Online]. Available: http://doi.acm.org/10.1145/1183287.1183290

[3] J. Ma, J. Zhao, J. Tian, A. L. Yuille, and Z. Tu, "Robust point matching via vector field consensus," *IEEE Transactions on Image Processing*, vol. 23, no. 4, pp. 1706–1721, 2014. [Online]. Available: http://dx.doi.org/10.1109/TIP.2014.2307478

[4] M. Smolik, V. Skala, and Z. Majdisova, "Vector field radial basis function approximation," *Advances in Engineering Software*, vol. 123, pp. 117–129, 2018.

[5] M. Smolik, V. Skala, and M. Zuzana, "3D vector field approximation and critical points reduction using radial basis functions," in *International Conference on Applied Physics, System Science and Computers*. Springer, 2018, pp. 1–6.

[6] D. Zotov, A. Shurup, and O. Rumyantseva, "Vector field reconstruction of flows using the novikov–agaltsov functional algorithm and the additive correlation method," *Bulletin of the Russian Academy of Sciences: Physics*, vol. 81, no. 1, pp. 101–105, 2017.

[7] L. Bonaventura, A. Iske, and E. Miglio, "Kernel-based vector field reconstruction in computational fluid dynamic models," *International Journal for Numerical Methods in Fluids*, vol. 66, no. 6, pp. 714–729, 2011.

[8] D. Schlipf, A. Rettenmeier, F. Haizmann, M. Hofsäß, M. Courtney, and P. W. Cheng, "Model based wind vector field reconstruction from lidar data," 2012.

[9] A. Borraccino, D. Schlipf, F. Haizmann, and R. Wagner, "Wind field reconstruction from nacelle-mounted lidars short range measurements," *Wind Energy Science Discussions*, vol. 2, pp. 269–283, 2017.

[10] M. Lage, F. Petronetto, A. Paiva, H. Lopes, T. Lewiner, and G. Tavares, "Vector field reconstruction from sparse samples with applications," in *2006 19th Brazilian Symposium on Computer Graphics and Image Processing*. IEEE, 2006, pp. 297–306.

[11] L. Wei-Dong, K. Ren, S. Meunier-Guttin-Cluzel, and G. Gouesbet, "Global vector-field reconstruction of nonlinear dynamical systems from a time series with svd method and validation with lyapunov exponents," *Chinese Physics*, vol. 12, no. 12, p. 1366, 2003.

[12] D. Frakes, M. Smith, D. De Zélicourt, K. Pekkan, and A. Yoganathan, "Three-dimensional velocity field reconstruction," *Journal of biomechanical engineering*, vol. 126, no. 6, pp. 727–735, 2004.

[13] P. Towers and B. L. Jones, "Real-time wind field reconstruction from lidar measurements using a dynamic wind model and state estimation," *Wind Energy*, vol. 19, no. 1, pp. 133–150, 2016.

[14] H. Braun and A. Hauck, "Tomographic reconstruction of vector fields," *IEEE Transactions on signal processing*, vol. 39, no. 2, pp. 464–471, 1991.

[15] R. Pan and V. Skala, "A two-level approach to implicit surface modeling with compactly supported radial basis functions," *Engineering with Computers*, vol. 27, no. 3, pp. 299–307, 2011.

[16] M. Smolik and V. Skala, "Large scattered data interpolation with radial basis functions and space subdivision," *Integrated Computer-Aided Engineering*, vol. 25, no. 1, pp. 49–26, 2018.

[17] G. E. Fasshauer, *Meshfree approximation methods with MATLAB*. World Scientific, 2007, vol. 6.

[18] V. Skala, "Meshless interpolations for computer graphics, visualization and games," in *Eurographics 2015 - Tutorials, Zurich, Switzerland, May 4-8, 2015*, 2015. [Online]. Available: http://dx.doi.org/10.2312/egt.20151046

[19] R. L. Hardy, "Multiquadric equations of topography and other irregular surfaces," *Journal of geophysical research*, vol. 76, no. 8, pp. 1905–1915, 1971.

[20] I. Schagen, "Interpolation in two dimensions—a new technique," *IMA Journal of Applied Mathematics*, vol. 23, no. 1, pp. 53–59, 1979.

[21] B. Fornberg and C. Piret, "On choosing a radial basis function and a shape parameter when solving a convective PDE on a sphere," *J. Comput. Physics*, vol. 227, no. 5, pp. 2758–2780, 2008. [Online]. Available: http://dx.doi.org/10.1016/j.jcp.2007.11.016

[22] H. Wendland, "Computational aspects of radial basis function approximation," *Studies in Computational Mathematics*, vol. 12, pp. 231–256, 2006.

[23] K. Uhlir and V. Skala, "Radial basis function use for the restoration of damaged images," in *Computer vision and graphics*. Springer, 2006, pp. 839–844.

[24] Y. Yokoi and R. Vitkovičová, "Experimental investigation of the mutual interference flow of two circular cylinders by flow visualization," in *EPJ Web of Conferences*, vol. 143. EDP Sciences, 2017, p. 02146.